Journal of Luminescence 225 (2020) 117392

Contents lists available at ScienceDirect

Journal of Luminescence

journal homepage: http://www.elsevier.com/locate/jlumin

Near-infrared photoluminescence and phosphorescence properties of Cr^{3+}-Doped garnet-type $Y_3Sc_2Ga_3O_{12}$

Xian Yang [a,1], Weibin Chen [b,1], Dongsheng Wang [a], Xirong Chai [a], Gening Xie [b], Zhiguo Xia [c], Maxim S. Molokeev [d], Yingliang Liu [b,e], Bingfu Lei [a,b,e,*]

[a] Guangdong Laboratory of Lingnan Modern Agriculture, College of Horticulture, South China Agricultural University, Guangzhou, 510642, PR China
[b] Key Laboratory for Biobased Materials and Energy of Ministry of Education, Guangdong Provincial Engineering Technology Research Center for Optical Agriculture, College of Materials and Energy, South China Agricultural University, Guangzhou, 510642, PR China
[c] State Key Laboratory of Luminescent Materials and Devices and Institute of Optical Communication Materials, South China University of Technology, 510641, Guangzhou, PR China
[d] Laboratory of Crystal Physics, Kirensky Institute of Physics, Federal Research Center KSC SB RAS, Krasnoyarsk, 660036, Russia
[e] Guangdong Laboratory of Lingnan Modern Agriculture, Guangzhou, 510642, PR China

ARTICLE INFO

Keywords:
Garnet-type phosphor
Near infrared
Phosphorescence emission
Thermoluminescence

ABSTRACT

Garnet-type $Y_3Sc_2Ga_3O_{12}:Cr^{3+}$ phosphor has been synthesized by a solid-state reaction. XRD result revealed the successful phase formation and Cr^{3+} doping in $Y_3Sc_2Ga_3O_{12}$. The excitation spectrum at about 260, 450, and 630 nm corresponded to three spin-allowed Cr^{3+} *d-d* intra-transitions of $^4A_2$-$^4T_1$ (^4P), $^4A_2$-$^4T_1$ (^4F), and $^4A_2$-$^4T_2$ (^4F), respectively, among which the near infrared (NIR) emission peak at around 740 nm is identified. Moreover, the phosphorescence emission property, thermoluminescence and related luminescence mechanisms are discussed as well. The fabricated NIR phosphor-converted light-emitting diodes (pc-LEDs) suggest its potential of $Y_3Sc_2Ga_3O_{12}:Cr^{3+}$ phosphor for non-visible light source application.

1. Introduction

Persistent phosphors in visible region have been well developed and have been widely applied in various important fields as security signs, emergency route signage, identification makers, or media diagnostics [1,2]. Comparatively, the research and development of persistent phosphors in the near infrared (NIR) region are lacking, even though there are growing demands for applications as identification makers in defense and security and as optical probes in bio-imaging [3,4]. The NIR persistent phosphors have been reported such as lanthanide or transition metal doped garnet and spinel in very recent years, as reported by Tabane's group [5,6], with the afterglow times ranging from several minutes to several hours after excitation by ultraviolet light [7,8]. During the design of NIR phosphors, trivalent chromium ion (Cr^{3+}) is a favorable luminescent center is solids since its $3d^3$ electron configuration allows a narrow-band emission (usually near 700 nm) due to the spin-forbidden ^2E-$^4A_2$ transition, or a broadband emission (650–1600 nm) ascribing to the spin-allowed $^4T_2$-$^4A_2$ transition, which strongly depends on the crystal-field environment of the host lattices [9,10]. Here, we comparatively reported the NIR photoluminescence and phosphorescence properties of Cr^{3+}-doped garnet-type phosphor, $Y_3Sc_2Ga_3O_{12}:Cr^{3+}$, and their emission mechanism and non-visible light source applications have been demonstrated.

The crystal structure of $Y_3Sc_2Ga_3O_{12}$ was evolved from famous garnet phase, $Y_3Al_5O_{12}$, by the iso-structural replacement of Sc/Al and Ga/Al atoms. $Y_3Sc_2Ga_3O_{12}$ possess a cubic crystal structure and a space group $Ia\bar{3}d$ with lattice parameters of $a = b = c = 12.47$ Å [11]. Up to now, rare earth and transition metal doped $Y_3Sc_2Ga_3O_{12}$ have been extensively investigated over the last few decades. For example, Kück et al. investigated the excited state absorption and its influence on the laser behaviour of $Y_3Sc_2Ga_3O_{12}:Cr^{4+}$ [12]. Herein, we demonstrated the phase formation, NIR photoluminescence and phosphorescence properties of $Y_3Sc_2Ga_3O_{12}:Cr^{3+}$ phosphors to give new insight into the potential applications.

* Corresponding author. Guangdong Laboratory of Lingnan Modern Agriculture, College of Horticulture, South China Agricultural University, Guangzhou, 510642, PR China.
E-mail address: tleibf@scau.edu.cn (B. Lei).
[1] These authors have contributed equally to this work.

https://doi.org/10.1016/j.jlumin.2020.117392
Received 22 January 2020; Received in revised form 23 April 2020; Accepted 17 May 2020
Available online 19 May 2020

2. Experimental section

$Y_3Sc_2Ga_3O_{12}:Cr^{3+}$ phosphors were synthesized by high temperature solid-state reaction, starting from a mixture containing Y_2O_3 (99.995%), Sc_2O_3 (99.995%), Ga_2O_3 (99.995%), BaF_2 (99.995%) and Cr_2O_3 (99.995%) in the given stoichiometric proportions with the 5% BaF_2 as flux, and the addition of BaF_2 flux will benefit to the improvement in the crystalline property and luminescence intensity. After mixing and grinding, the mixtures were placed into an alumina crucible and then fired in air at 1520 °C for 5 h. After this, the samples were furnace-cooled to room temperature, ground again into powder and then sift to make sure the size is ~30 μm for the following measurement.

The powder X-ray diffraction (XRD) measurements were conducted on a D8 Advance diffractometer (Bruker Corporation, Germany) operating at 40 kV and 40 mA with Cu Kα radiation (λ = 0.15406 Å). Room temperature excitation and emission spectra were measured on a fluorescence spectrophotometer (F-4600, HITACHI, Japan) with 5 nm slits and a photomultiplier tube operating at 400 V, a 150 W Xe lamp used as the excitation lamp. Before we can measure the afterglow emission spectra, the samples were firstly irradiated for 15 min with a 12 W, 365 nm UV lamp (The radiation distance is fixed at 10 cm), after that they are measured on the same F-4600 fluorescence spectrophotometer. The TL spectra were recorded by using microcomputer TL dosimeters (FJ427-A1, Beijing Nuclear Instrument Factory, Beijing, China.).

3. Results and discussion

XRD patterns of the as-prepared $Y_3Sc_2Ga_3O_{12}:Cr^{3+}$ phosphors were collected to verify the phase purity. As is given in Fig. 1a, one can see that the diffraction peaks of the as-prepared sample are basically indexed to the corresponding standard data for cubic phase of $Y_3Sc_2Ga_3O_{12}$ (JCPDS 25–1246. Fig. 1b gives the representative diagram of the $Y_3Sc_2Ga_3O_{12}$ unit cell, which belongs to the cubic $A_3B_2C_3X_{12}$-type structure with the space group $Ia\bar{3}d$ [11,13]. This structure can be described as a network of [GaO_4] tetrahedral and [ScO_6] octahedral linked by shared oxygen ions at the corner. The polyhedra are arranged in chains along the three crystallographic directions and form dodecahedral cavities occupied by the Y^{3+} ions. Additionally, Considering the high tolerability of these three cation sites, the larger dodecahedral sites are ideal for lanthanide ions, while the smaller octahedral sites are of the appropriate size for Cr^{3+} ions [14]. The similarity of ionic radii of Sc^{3+} (0.885 Å) and Cr^{3+} (0.755 Å) ions as well as their identical charge and similar electronegativity all favor Cr^{3+} substitution on the octahedral Sc^{3+} site [15].

Trivalent chromium ions belong to 3 d^3 electronic configurations and in octahedral symmetry the splitting of the energy levels can be explained by Tanabe-Sugano energy level diagram as shown in Fig. 2a. The d^3 configuration gives rise to two quartet terms and ^4F and ^4P with ^4F term lying lower to ^4P as per Hund's rule. In addition to these quartet terms, there are several doublet terms. The ^2G term splits into ^2E level, and the $^4A_2$, $^4T_2$, and $^4T_1$ levels come from the 4F term [16,17].

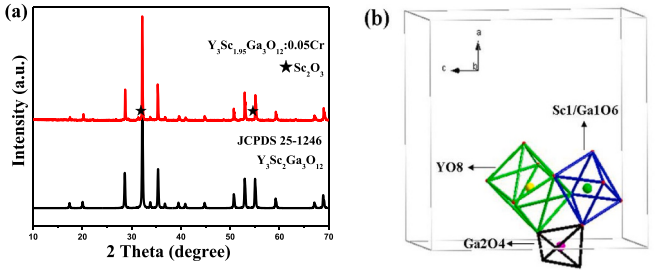

Fig. 1. (a) XRD pattern of $Y_3Sc_{1.95}Ga_3O_{12}:0.05Cr^{3+}$ sample and the standard pattern of JCPDS 25–1246, and minor impurity has been also marked. (b) Unit cell of $Y_3Sc_2Ga_3O_{12}$ crystal and the different polyhedra.

Moreover, the two distinct luminescence behaviors are depending on the crystal field: (1) broad band emission ($^4T_2$-$^4A_2$ transition) for 10Dq ≪ $10Dq_{ESCO}$ in the weak field sites (ESCO means the excited state cross over), and (2) narrow R lines emission (^2E-$^4A_2$ transition) for 10Dq ≫ $10Dq_{ESCO}$ in the strong crystal field sites. In addition, the borderline between the strong and weak fields is known as the intermediate field region, which is shown in Fig. 2b as a configurational coordinate diagram.

Fig. 3 shows the normalized excitation and emission spectra of $Y_3Sc_{1.95}Ga_3O_{12}:0.05Cr^{3+}$ at room temperature. The PLE spectra monitored at 740 nm covers a very broad spectral region (from 400 to 700 nm) and consists of three main excitation bands originating from the inner transitions of Cr^{3+}, including the 260 nm band originating from the $^4A_2 \rightarrow {}^4T_1$ (^4P) transition, the 450 nm band originating from the $^4A_2 \rightarrow {}^4T_1$ (^4F) transition and 630 nm band originating from the $^4A_2 \rightarrow {}^4T_2$ (^4F) transition. Under excitation at about 450 nm, the material produce a strong and broad NIR emission band which covers from 650 to 900 nm with maxima at around 740 nm. According to the crystal field estimation, the specific value is shown in Table 1, $Y_3Sc_2Ga_3O_{12}:Cr^{3+}$ belongs to the intermediate field region. The broadband emission may be ascribed to the $^4T_2 \rightarrow {}^4A_2$ transition from some disordered Cr^{3+} in this host system, whereas the broadening of the $^2E \rightarrow {}^4A_2$ emission is probably caused by the electron-phonon coupling [18,19].

Fig. 4 presents the photoluminescence emission (λ_{ex} = 450 nm) spectra of the $Y_3Sc_{2-x}Ga_3O_{12}:xCr^{3+}$ phosphors with different concentrations of Cr^{3+} (ranging from 0.01 to 0.20) at room temperature. As is shown in Fig. 4a, this series of samples all produce a broad-band NIR emission with a peak at around 740 nm, and the emission spectra have no obvious changes in the spectra configuration except for the emission intensity. Moreover, a red-shift tendency from 740 nm to 750 nm is observed as the concentration of Cr^{3+} increase gradually which can be clearly seen in Fig. 4b.

As a comparison, the spectral shapes of photoluminescence and persistent luminescence in $Y_3Sc_{1.99}Ga_3O_{12}:0.01Cr^{3+}$ was contrasted as demonstrated in Fig. 5a. From the picture we can cee that the afterglow emission spectra exhibit a similar broad band as the photoluminescence spectrum, which is also attributed to the typical emission of Cr^{3+} ion. Fig. 5b shows the phosphorescence spectra of this series of samples of $Y_3Sc_{2-x}Ga_3O_{12}:xCr^{3+}$ (x = 0.01, 0.03, 0.05, 0.10, 0.15 and 0.20). With increasing Cr^{3+} concentration, the emission intensity firstly increases, and reaches the maximum when the concentration of Cr^{3+} is 0.05, and then the afterglow emission intensity decrease with further increasing concentration. This phenomenon is different from the PL spectra at room temperature which is caused by the different trap level in the host when the concentration of Cr^{3+} changes. As we know, the change of the emission peak wavelengths can be attributed to the change of the Cr^{3+} energy level, which is easy to be influenced by the crystal lattice. For example, the crystal field strength of Cr^{3+} in Ga^{3+} site will be stronger [14]. A schematic diagram depicting of all the related energy levels was shown in Fig. 6, and it is clear to find that the defect energy level plays important role in the NIR persistent emission.

In order to further investigate the reason for the improving afterglow property and provide the experimental data for the study of afterglow emission mechanism, we have used thermoluminescence (TL) measurement. By using TL technique, it is easier to evaluate the density and depth of traps generated in materials under the irradiation of UV light, and the peaks in the TL curve represent the depth and the density of traps [20,21]. It is normal that the energy stored in the excessive shallow traps will released at a very fast ratio under room temperature thermal balance the energy stored in a relatively deep trap cannot return to the excited state under room temperature for the reason that the electrons have been strongly immobilized in trap [22]. Therefore, appropriate traps are important to create phosphorescence emission. As is reported in the previous work, the ideal trap depth for excellent long persistent luminescence was reported at 0.6–0.7 eV [23]. In order to get further information about the traps and detect the trapping levels, TL flow curve

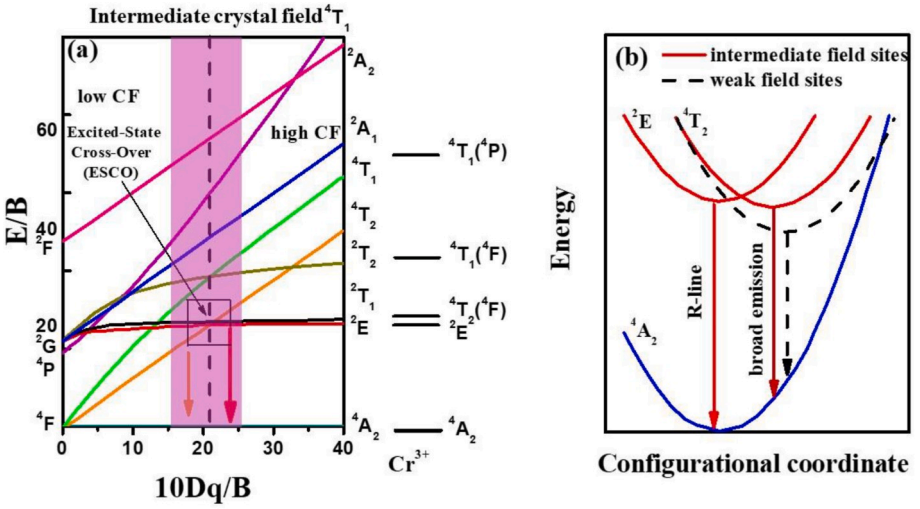

Fig. 2. (a) Tunabe-sugnano diagram for Cr^{3+} in $Y_3Sc_2Ga_3O_{12}$ and the corresponding energy levels and transitions have been given. (b) Mechanistic configurational coordinate diagram illustrating different emission channels for the Cr^{3+} dopant.

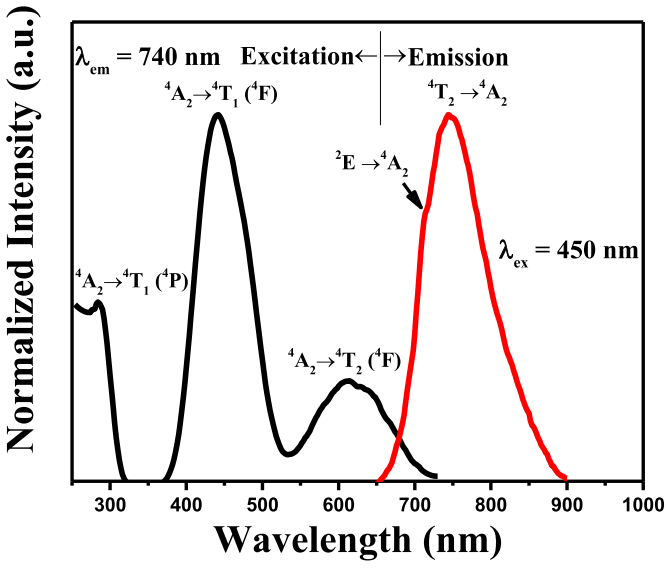

Fig. 3. Normalized excitation and emission spectra of $Y_3Sc_{1.95}Ga_3O_{12}$:0.05Cr^{3+} phosphor at room temperature with the corresponding monitoring wavelength (740 nm) for excitation spectrum and excitation wavelength (450 nm) for emission spectrum.

Table 1
Estimated crystal field parameters of $Y_3Sc_2Ga_3O_{12}$:0.05Cr^{3+}.

Transition/Parameter	$Y_3Sc_2Ga_3O_{12}$:0.05Cr^{3+}
E ($^4A_2 \rightarrow {}^4T_1$ (^4F))	450 nm/22,222 cm^{-1}
E ($^4A_2 \rightarrow {}^4T_2$ (^4F))	630 nm/15,873 cm^{-1}
Dq	1587 cm^{-1}
B	635 cm^{-1}
10*Dq*/*B*	25.0

of these phosphors are recorded. Fig. 7 shows the TL curves of $Y_3Sc_{1.95}Ga_3O_{12}$:0.05Cr^{3+} sample (without baseline). For $Y_3Sc_{1.95}Ga_3O_{12}$:0.05Cr^{3+}, only one peak is observed above room temperature, which resides around the temperature of 360 K. For the sake of clarifying the traps, a method provided by Chen is used to obtain the TL parameters by fitting experimental data according to the general order kinetics formula [24]. Two deconvoluted bands are denotes as band 1 and band 2, respectively, and the depth values of each individual band ban be calculated by the following Eq. (1) [25],

$$E = T_m/500 \quad (1)$$

Where E is the activation energy which stands for the activation energy which means the trap depth; T_m is the temperature of corresponding TL peaks. The calculated value of trap depths (E) of $Y_3Sc_{1.95}Ga_3O_{12}$:0.05Cr^{3+} is determined to be 0.72 eV with T_m of 360 K. It is reported that the TL bands are situates somewhere between 350 and 420 K if the materials show excellent phosphorescence performance [26].

In order to explore the application of NIR-emitting $Y_3Sc_{1.95}Ga_3O_{12}$:0.05Cr^{3+} phosphor, a phosphor-converted light-emitting diode (pc-LED) was fabricated by combining the as-prepared NIR phosphor and the commercial blue light-emitting chip (450 nm). The broad-band PL spectrum of LED device upon different forward bias currents (20–120 mA) and the as-obtained NIR pc-LED lamps are given in Fig. 8a. Unfortunately, we can only obtain data before 780 nm due to the limitation of detection range. Moreover, Fig. 8b shows the photographs obtained by different cameras under natural light and NIR pc-LED light, respectively. And the distance from the white paper to the NIR pc-LED light is 180 cm. Nothing can be detected by NIR camera once the NIR pc-LED is off. In contrast, the NIR camera can capture black-and-white images while the NIR pc-LED lamp is lighted, and the letter "E" on the white paper is also clearly visible. These results indicate the application of the $Y_3Sc_{1.95}Ga_3O_{12}$:0.05Cr^{3+} phosphor in night-vision technologies.

4. Conclusion

In summary, we have successfully synthesized single-phased $Y_3Sc_2Ga_3O_{12}$:Cr^{3+} phosphor with NIR photoluminescence and phosphorescence emissions. The as-prepared phosphor show strong and broad-band NIR emission band ranging from 650 to 900 nm with maxima at around 740 nm under the excitation of 450 nm. The afterglow emission spectra reveal that the optimum doping concentration of Cr^{3+} and the corresponding luminescence mechanism has been investigated. Moreover, the fabricated NIR pc-LEDs by using the $Y_3Sc_{1.95}Ga_3O_{12}$:0.05Cr^{3+} phosphor demonstrates its potential application in non-visible light source.

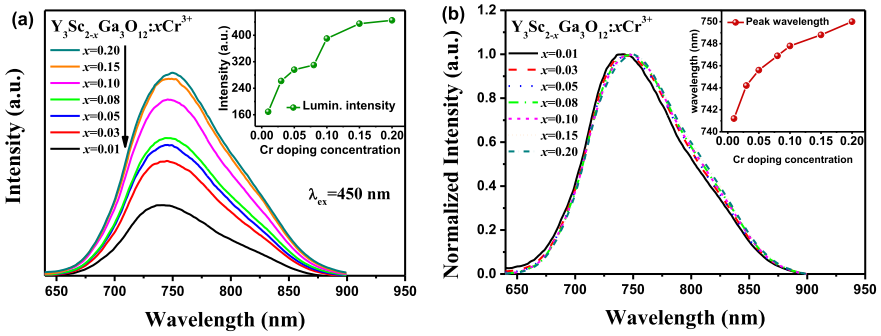

Fig. 4. (a) PL spectra and (b) Normalized emission spectra of $Y_3Sc_{2-x}Ga_3O_{12}:xCr^{3+}$ (x = 0.01, 0.03, 0.05, 0.08, 0.10, 0.15 and 0.20), and insets present the functions of photoluminescence intensity and peak wavelength with Cr doping concentration.

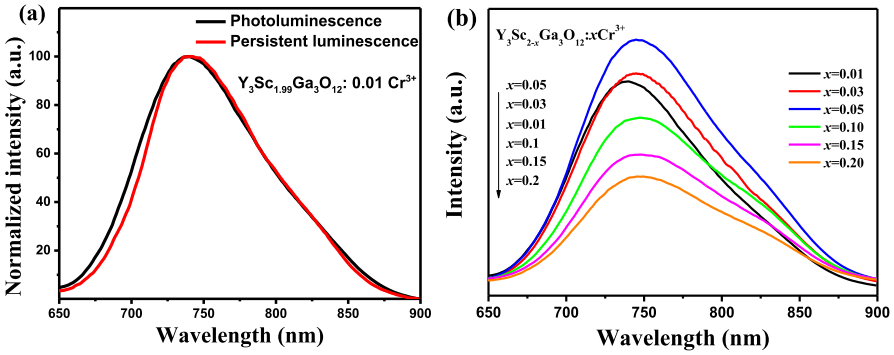

Fig. 5. (a) The comparison of spectral shapes obtained by photoluminescence and persistent luminescence in $Y_3Sc_{1.99}Ga_3O_{12}$:0.01Cr^{3+}. (b) Afterglow emission spectra of $Y_3Sc_{2-x}Ga_3O_{12}:xCr^{3+}$ (x = 0.01, 0.03, 0.05, 0.10, 0.15 and 0.20).

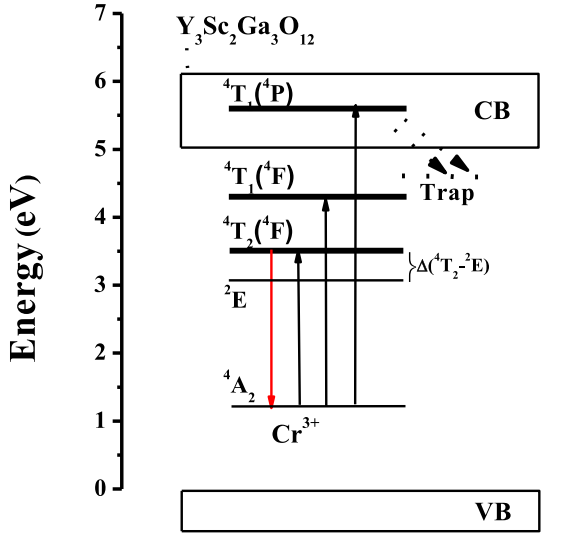

Fig. 6. Schematic energy level diagram for Cr^{3+} in $Y_3Sc_{1.95}Ga_{3-y}Al_yO_{12}$:0.05$Cr^{3+}$ phosphors.

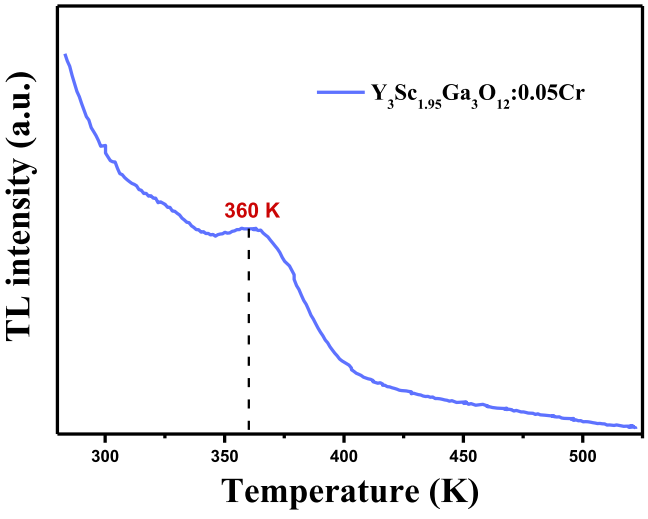

Fig. 7. TL curves of $Y_3Sc_{1.95}Ga_3O_{12}$:0.05Cr^{3+} sample. (without baseline).

Declaration of competing interest

The authors declare that they have no known competing financial interests or personal relationships that could have appeared to influence the work reported in this paper.

CRediT authorship contribution statement

Xian Yang: Data curation, Methodology, Visualization, Writing - original draft. **Weibin Chen:** Data curation, Project administration, Writing - original draft. **Dongsheng Wang:** Investigation. **Xirong Chai:** Validation. **Gening Xie:** Funding acquisition. **Zhiguo Xia:** Writing - review & editing. **Maxim S. Molokeev:** Formal analysis. **Yingliang Liu:** Funding acquisition, Conceptualization, Methodology, Software. **Bingfu Lei:** Funding acquisition, Conceptualization, Methodology, Resources,

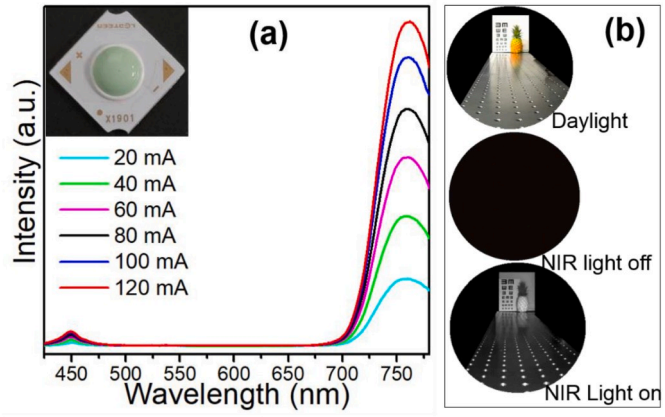

Fig. 8. (a) PL spectra of the as-fabricated phosphor-converted-LED upon various forward bias currents. (b) Photographs taken by a visible camera in the daylight and a NIR camera under light off and light on states of the NIR pc-LED light, respectively.

Supervision.

Acknowledgments

The present work was supported by the National Natural Science Foundations of China (Grant No. 21671070); the Project of GDUPS (2018) for Prof. Bingfu LEI; the Guangzhou Science & Technology Project, China (No. 201704030086); and the National Undergraduate Innovation and Entrepreneurship Training Program granted for Gening Xie (No. 201910564035).

Appendix A. Supplementary data

Supplementary data to this article can be found online at https://doi.org/10.1016/j.jlumin.2020.117392.

References

[1] J. Hölsä, Persistent luminescence beats the afterglow: 400 Years of persistent luminescence, The Electrochemical Society Interface 18 (2009) 42–45.
[2] W.M. Yen, Practical Applications of Phosphors, CRC Press, Boca Raton, 2007.
[3] Q.M. Chermont, C. Chanéac, J. Seguin, et al., Nanoprobes with near-infrared persistent luminescence for in vivo imaging, Proc. Natl. Acad. Sci. Unit. States Am. 104 (2007) 9266–9271.
[4] L. Liang, N. Chen, Y. Jia, Q. Ma, J. Wang, Q. Yuan, W. Tan, Recent progress in engineering near-infrared persistent luminescence nanoprobes for time-resolved biosensing/bioimaging, Nano Research 12 (2019) 1279–1292.
[5] J. Xu, S. Tanabe, A.D. Sontakke, J. Ueda, Near-infrared multi-wavelengths long persistent luminescence of Nd^{3+} ion through persistent energy transfer in Ce^{3+}, Cr^{3+} co-doped $Y_3Al_2Ga_3O_{12}$ for the first and second bio-imaging windows, Appl. Phys. Lett. 107 (2015), 081903.
[6] J. Xu, J. Ueda, S. Tanabe, Novel persistent phosphors of lanthanide–chromium co-doped yttrium aluminum gallium garnet: design concept with vacuum referred binding energy diagram, J. Mater. Chem. C 4 (2016) 4380–4386.
[7] Z. Pan, Y. Lu, F. Liu, Sunlight-activated long-persistent luminescence in the near-infrared from Cr^{3+}-doped zinc gallogermanates, Nat. Mater. 11 (2011) 58–63.
[8] Y. Li, Y. Li, K. Sharafudeen, G.-P. Dong, S.F. Zhou, Z.J. Ma, M.Y. Peng, J.R. Qiu, A strategy for developing near infrared long-persistent phosphors: taking $MAlO_3$:Mn^{4+},Ge^{4+} (M = La, Gd) as an example, J. Mater. Chem. C 2 (2014) 2019–2027.
[9] Y. Li, S. Zhou, Y. Li, K. Sharafudeen, Z. Ma, G. Dong, M. Peng, J. Qiu, Long persistent and photo-stimulated luminescence in Cr^{3+}-doped Zn–Ga–Sn–O phosphors for deep and reproducible tissue imaging, J. Mater. Chem. C 2 (2014), 2657-2633.
[10] H. Zeng, T. Zhou, L. Wang, R. Xie, Two-site occupation for exploring ultra-broadband near-infrared phosphor—double-perovskite La_2MgZrO_6:Cr^{3+}, Chem. Mater. 31 (2019) 5245–5253.
[11] W. Isaacs, Crystal data for yttrium-indium-gallium and yttrium-scandium-gallium garnets, J. Appl. Crystallogr. 6 (1973) 416–417.
[12] K. Kück, S. Hartung, K. Petermann, G. Huber, Excited state absorption and its influence on the laser behavior of Cr^{4+} -doped garnets, J. Lumin. 72–74 (1997) 222–223.
[13] Y. Luo, Z. Xia, Effect of Al/Ga substitution on photoluminescence and phosphorescence properties of garnet-type $Y_3Sc_2Ga_{3-x}Al_xO_{12}$:$Ce^{3+}$ phosphor, J. Phys. Chem. C 118 (2014) 23297–23305.
[14] J. Xu, J. Ueda, S. Tanabe, Toward tunable and bright deep-red persistent luminescence of Cr^{3+} in garnets, J. Am. Ceram. Soc. 100 (2017) 4033–4044.
[15] B. Malysa, A. Meijerink, T. Jüstel, Temperature dependent Cr^{3+} photoluminescence in garnets of the type $X_3Sc_2Ga_3O_{12}$ (X = Lu, Y, Gd, La), J. Lumin. 202 (2018) 523–531.
[16] I. Hernández, F. Rodríguez, A. Tressaud, Optical properties of the $(CrF_6)_3$- complex in A_2BMF_6:Cr^{3+} elpasolite crystals: variation with M-F bond distance and hydrostatic pressure, Inorg. Chem. 47 (2008) 10288–10298.
[17] J. Zhou, Z. Xia, Synthesis and near-infrared luminescence of $La_3GaGe_5O_{16}$:Cr^{3+} phosphors, RSC Adv. 4 (2014) 46313–46318.
[18] W. Huang, C. Cheng, Z. Bao, C. Yang, K. Lu, C. Kang, C. Lin, R. Liu, Broadband Cr^{3+}, Sn^{4+} -doped oxide nanophosphors for infrared mini light-emitting diodes, Angew. Chem. Int. Ed. 58 (2019) 2069–2072.
[19] C. Liu, Z. Xia, M. Chen, M.S. Molokeev, Q. Liu, Near-infrared luminescence and color tunable chromophores based on Cr^{3+}-doped mullite-type $Bi_2(Ga,Al)_4O_9$ solid solutions, Inorg. Chem. 54 (2015) 1876–1882.
[20] D. Xu, Z. Qiu, Q. Zhang, L. Huang, Y. Ye, L. Cao, J. Meng, Sr_2MgWO_6:Cr^{3+} phosphors with effective near-infrared fluorescence and long-lasting phosphorescence, J. Alloys Compd. 781 (2019) 473–478.
[21] J. Du, D. Poelman, Near-infrared persistent luminescence in Mn^{4+} doped perovskite type solid solutions, Ceram. Int. 45 (2019) 8345–8353.
[22] Y. Gong, Y. Wang, Z. Jiang, X. Xu, Y. Li, Luminescent properties of long lasting phosphor $Ca_2MgSi_2O_7$:Eu^{2+}, Mater. Res. Bull. 44 (2009) 1916–1919.
[23] T. Matsuzawa, Y. Aoki, N. Takeuchi, Y. Murayama, A new long phosphorescent phosphor with high brightness, $SrAl_2O_4$:Eu^{2+}, Dy^{3+}, J. Electrochem. Soc. 143 (1996) 2670–2673.
[24] R. Chen, Glow curves with general order kinetics, J. Electrochem. Soc. 116 (1969) 1254–1257.
[25] R. Chen, On the calculation of activation energies and frequency factors from glow curves, J. Appl. Phys. 40 (1969) 570–585.
[26] B. Lei, B. Li, H. Zhang, L. Zhang, Y. Cong, W. Li, Synthesis and luminescence properties of cube-structured $CaSnO_3$/RE^{3+}, RE =(Pr, Tb) long-lasting phosphors, J. Electrochem. Soc. 154 (2007) H623–H630.